JACS
JOURNAL OF THE AMERICAN CHEMICAL SOCIETY
pubs.acs.org/JACS
Article

Topological Design of Highly Anisotropic Aligned Hole Transporting Molecular Bottlebrushes for Solution-Processed OLEDs

Nari Kang,[⋈] Sangho Cho,[⋈] Eric E. Leonhardt,[⋈] Chun Liu, Stanislav V. Verkhoturov, William Henry Hunter Woodward, Michael J. Eller, Tianyu Yuan, Thomas C. Fitzgibbons, Yannick P. Borguet, Ashlee A. Jahnke, Anatoliy N. Sokolov, Travis McIntire, Carl Reinhardt, Lei Fang, Emile A. Schweikert, Liam Patrick Spencer, Guorong Sun,* Guohua Xie,* Peter Trefonas,* and Karen L. Wooley*

Cite This: *J. Am. Chem. Soc.* 2022, 144, 8084–8095

ABSTRACT: Polyvinyl polymers bearing pendant hole transport functionalities have been extensively explored for solution-processed hole transport layer (HTL) technologies, yet there are only rare examples of high anisotropic packing of the HT moieties of these polymers into substrate-parallel orientations within HTL films. For small molecules, substrate-parallel alignment of HT moieties is a well-established approach to improve overall device performance. To address the longstanding challenge of extension from vapor-deposited small molecules to solution-processable polymer systems, a fundamental chemistry tactic is reported here, involving the positioning of HT side chains within macromolecular frameworks by the construction of HT polymers having bottlebrush topologies. Applying state-of-the-art polymer synthetic techniques, various functional subunits, including triphenylamine (TPA) for hole transport and adhesion to the substrate, and perfluoro alkyl-substituted benzyloxy styrene for migration to the air interface, were organized with exquisite control over the composition and placement throughout the bottlebrush topology. Upon assembling the HT bottlebrush (HTB) polymers into monolayered HTL films on various substrates through spin-casting and thermal annealing, the backbones of HTBs were vertically aligned while the grafts with pendant TPAs were extended parallel to the substrate. The overall design realized high TPA π-stacking along the out-of-plane direction of the substrate in the HTLs, which doubled the efficiency of organic light-emitting diodes compared with linear poly(vinyl triphenylamine)s.

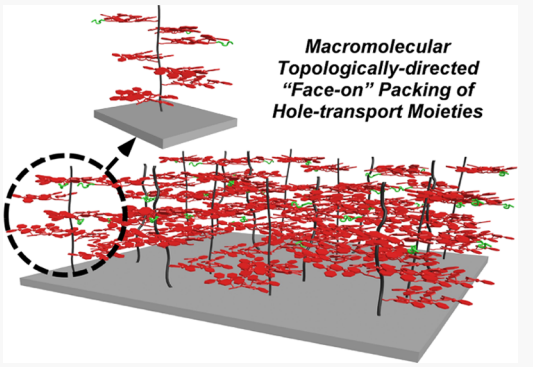

INTRODUCTION

It has been well established that the device performance (*e.g.*, efficiency, lifetime, and turn-on voltage) of a multilayered organic light-emitting diode (OLED) is dependent on the molecular composition and orientation within each layer and at each interlayer interface of the device, as these characteristics determine the charge mobility within the layers and the charge injection barrier levels between layers.[1−5] A high degree of alignment of planar molecules used as the hole injection layers (HILs), hole transport layers (HTLs), and electron transport layers (ETLs) into an anisotropic "face-on" orientation, *i.e.*, the charge transport moieties are aligned parallel to the substrate, has been shown to lower the hole injection barrier at the anode/HIL interface, to increase the hole mobility in the HTL[6−9] and electron mobility in the ETL.[10−12] Therefore, the molecular orientations relative to the substrate and within and between each layer are important for device performance.

Typically, orientation control of planar and quasiplanar π-conjugated small molecules is accomplished by vacuum deposition.[6−12] Although vacuum deposition techniques are capable of excellent orientational ordering,[13] they are limited by the molar masses that can be vaporized and the dimensions over which OLED devices can be fabricated. Solution processing could overcome these limitations, extending to macromolecular charge transport materials[14−18] and to large-scale dimensions. Unfortunately, except for conjugated polymers with long-range coplanarity,[19,20] solution processing of linear HT polymers bearing pendant charge transport functionalities[15,21−24] is incapable of achieving the exquisite

Received: January 12, 2022
Published: April 26, 2022

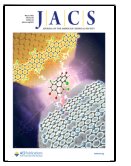

https://doi.org/10.1021/jacs.2c00420
J. Am. Chem. Soc. 2022, 144, 8084−8095

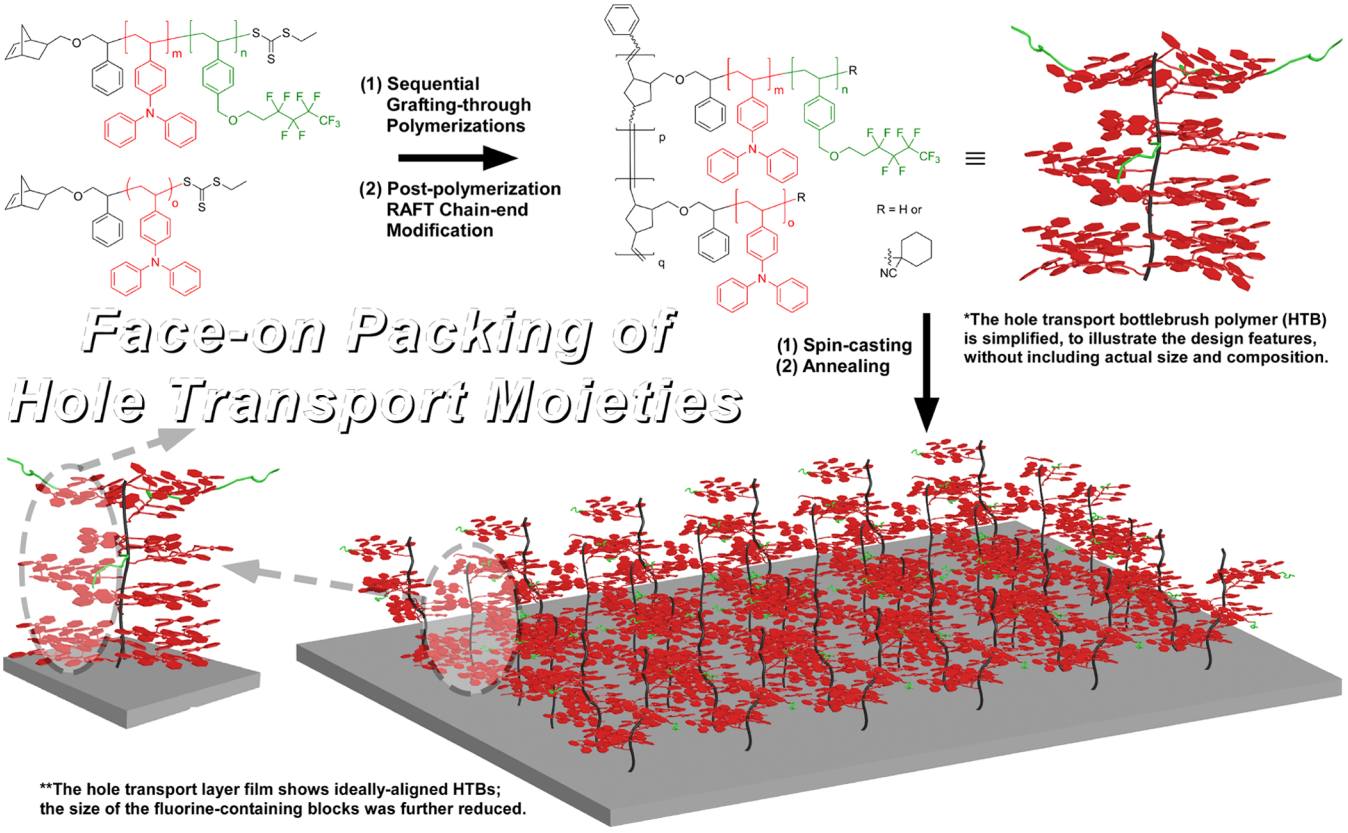

Figure 1. Schematic diagram of the overall design.

molecular ordering of evaporative methods due to the tendency for polymer chains to become kinetically trapped in suboptimal mixed moiety orientations during solvent evaporation, rather leading to unsatisfactory alignment of HT core units, and compromised device performance.[25] Therefore, the development of solution-processable polymeric hole transport materials that enable "face-on" packing of HT functionalities are highly desirable for technically simplified and cost-effective production of large-area OLED displays.

Introduction of the active functionalities topologically displayed within select regions of well-defined macromolecular frameworks, *e.g.*, a molecular bottlebrush architecture,[26−28] in concert with self-assembly processes, has been recognized as an effective strategy to afford innovative advanced materials. Bottlebrush polymers have demonstrated superiority over linear polymer counterparts in block copolymer lithography,[29,30] photonic,[31−33] photoresist,[34,35] superlubrication,[36,37] and biomedical[38,39] applications. We hypothesized that bottlebrush polymers in which the side chains/grafts contain pendant HT functional groups densely tethered along a relatively rigid backbone preferentially aligned normal to the substrate would facilitate preferential anisotropic "face-on" packing of HT functionalities within an HTL film. The strong size exclusion effect between side chains, in concert with an ordered alignment of the molecular brush backbones, was anticipated to decrease the inherent random coil conformation and chain entanglements of HT grafts[40,41] and provide pronounced confinement that would promote the cofacial packing between intergraft HT moieties. Thin-film assembly, through the use of surface-directing fluorinated moieties, spin-casting, and annealing-promoted vertical alignment of the molecular brushes on substrates,[34,35] was utilized as a strategy by which to place the HT units into an anisotropic horizontal orientation relative to the substrate. We address difficulties to achieve anisotropic packing of charge transport functionalities in solution-processed thin-film technologies by designing bottlebrush macromolecular structures that have active elements embedded within them, connected topologically within the macromolecular framework, as a fundamental chemistry tactic to address the longstanding challenge of aligning the hole transport moieties into preferential "face-on" orientations for advanced hole transport layer (HTL) technologies (Figure 1).

RESULTS AND DISCUSSION

Design and Syntheses of HT Bottlebrush Polymers. The HT bottlebrush (HTB) polymers utilized in this study were composed of two types of side chains, poly(4-vinyl triphenylamine)-*block*-poly(3,3,4,4,5,5,6,6,6-nonafluorohexyl-*para*-benzyloxy styrene) (PVTPA-*b*-PNFHBS) block copolymer and PVTPA homopolymer, in a block manner along a polynorbornene (PNB) backbone. Triphenylamines (TPAs) were employed as the HT functionalities. Triarylamines, in general, are an important class of small molecules for OLED applications that have been explored extensively, yet found to present challenges by the intrinsic propeller-like structure of the triarylamine moiety disrupting their anisotropic "face-on" packing within amorphous HTL films. The pendant TPA groups were also functioning for substrate adhesion, potentially through hydrogen-bonding, $\pi-\pi$ stacking, polar, electrostatic interactions, etc., with the various substrates. The fluorocarbon moieties in the PNFHBS block segments acted as surface energy-reducing functionalities to promote the vertical alignment of brushes on the substrate. In contrast to our previous

https://doi.org/10.1021/jacs.2c00420
J. Am. Chem. Soc. 2022, 144, 8084−8095

Scheme 1. Syntheses of Macromonomers (A) and HT Bottlebrushes (B)

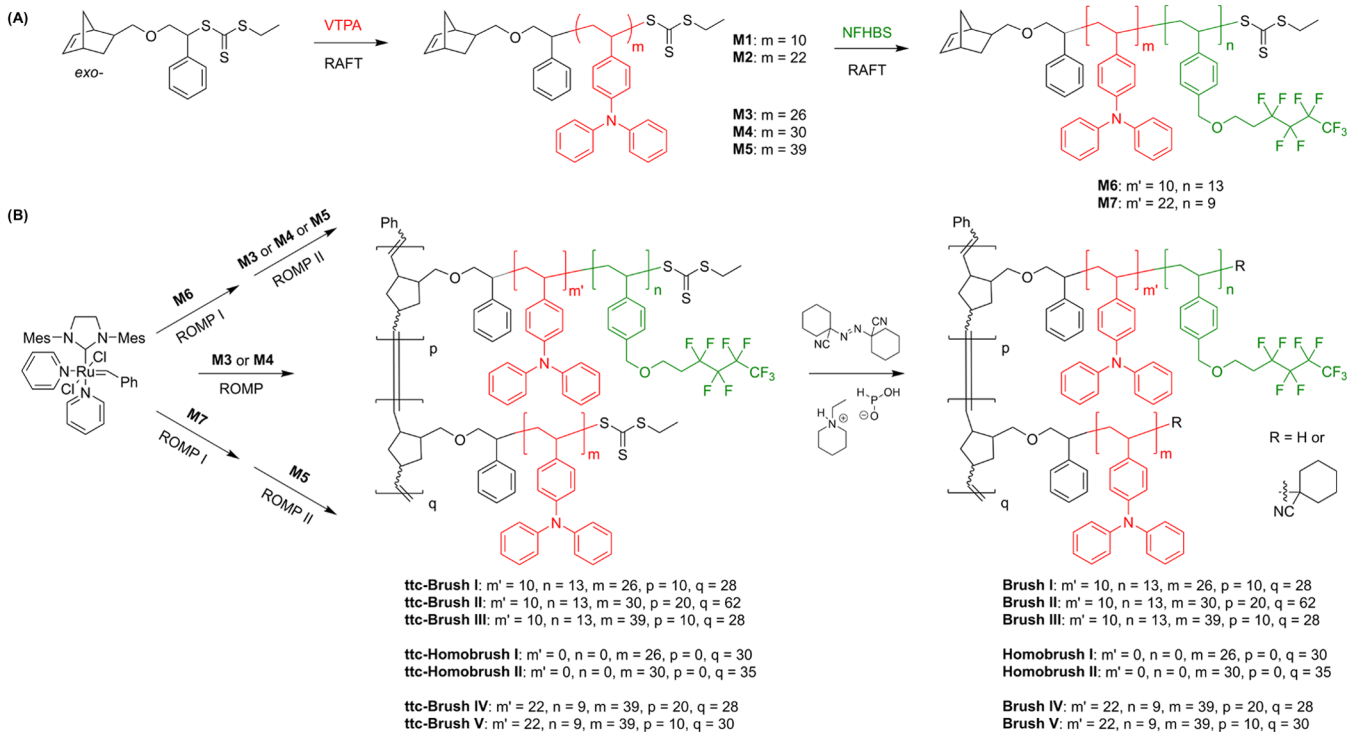

approaches,[34,35] the perfluorinated substituents were not directly connected to the TPA moieties. This design principle was applied due to the fact that density functional theory calculations of the highest occupied molecular orbital (HOMO) and the lowest unoccupied molecular orbital (LUMO) energy levels of small-molecule analogues, which represent fragments of the HTBs, showed noticeable decrease with the introduction of F-containing substituents on TPAs (Chart S1, entries 2−7 *vs* 1). Sequential "grafting-through" ring-opening metathesis polymerizations (ROMPs)[26−28] were utilized for the synthesis of the HTBs. Upon assembly of the HTBs into HTL films, the PNB backbones of individual brushes were perpendicularly oriented to the substrate, which could ideally provide a collective "face-on" packing of the TPAs within the HTL films.

An *exo*-NB-terminated trithiocarbonate chain transfer agent, with a stable ether linkage, was synthesized (Scheme S1 and Figure S1) and used for the preparation of the NB-(PVTPA-*b*-PNFHBS) and NB-PVTPA macromonomers (Scheme 1A, M1-M7) with predetermined molar masses and narrow dispersities ($Đ$ < 1.1) through reversible addition-fragmentation chain transfer (RAFT) polymerizations (Tables S1 and S2, Figures S2 and S3).[42−44] The well-defined structure of each macromonomer was verified through the combined data from spectroscopic and chromatographic analyses. Preservation of the characteristic NB and trithiocarbonate functionalities was confirmed by ^{1}H NMR spectroscopy. Molar mass calculations from ^{1}H NMR spectroscopy (comparing the peak integrals of NB alkenyl protons and aromatic protons) were consistent with size exclusion chromatography-multiangle light scattering (SEC-MALS) analyses (Tables S1 and S2).

A set of P[NB-*g*-(PVTPA-*b*-PNFHBS)]-*b*-P(NB-*g*-PVTPA) HTBs, with variable dimensions of overall molecular structure (Scheme 1B), was synthesized *via* sequential ROMPs of the corresponding macromonomers, using Grubbs' G3 catalyst. The progress of each ROMP was monitored by ^{1}H NMR spectroscopy and SEC (Figure S4) analyses of aliquots withdrawn at predetermined time points (Table S3). ^{1}H NMR spectra showed the disappearance of the NB alkenyl proton resonance at 6.08 ppm. Shifts of SEC peaks to shorter elution times were observed upon growth from macromonomers to bottlebrush polymers. As a note, we noticed the persistence of a SEC signal coinciding with *ca.* 5% of nonreacted macromonomers. This observation, together with a lack of remaining NB alkenyl proton resonance, suggested the presence of polymeric "contaminants" having an absence of terminal NB functionality, inherent to RAFT polymerizations. The degree of polymerization (DP) of the P[NB-*g*-(PVTPA-*b*-PNFHBS)] block was calculated based on the initial feed ratio of [catalyst]/[NB-(PVTPA-*b*-PNFHBS)] and ∼95% conversion during the first ROMP process. The relative DP_n ratios between the P[NB-*g*-(PVTPA-*b*-PNFHBS)] and P(NB-*g*-PVTPA) blocks were obtained based on ^{1}H NMR spectroscopy.

To reduce the potentially chemically reactive sites and enhance the thermal and long-term stabilities of HTLs in OLED devices, the trithiocarbonate RAFT functionalities were removed through a radical-induced reduction[45] to afford **Brush I−V**, as confirmed by the disappearance of the ethyl proton resonances (−SCH_2CH_3 at *ca.* 3.24 and 1.22 ppm, respectively, Figure S5). The SEC profiles of the final HTBs revealed slightly broadened molar mass distributions, which were attributed to the formation of potential intrabrush loops between side chains during the RAFT chain-end removal process, due to undesirable radical couplings. Semipreparative $CHCl_3$-SEC was applied to remove the defected brush and unreacted macromonomer "contaminates", as exemplified by **Brush II** (Figure S6a). Nevertheless, the relatively lower recovery yield (*ca.* 30%), as well as the appearance of a pronounced high molar mass shoulder of the SEC-purified

https://doi.org/10.1021/jacs.2c00420
J. Am. Chem. Soc. 2022, 144, 8084−8095

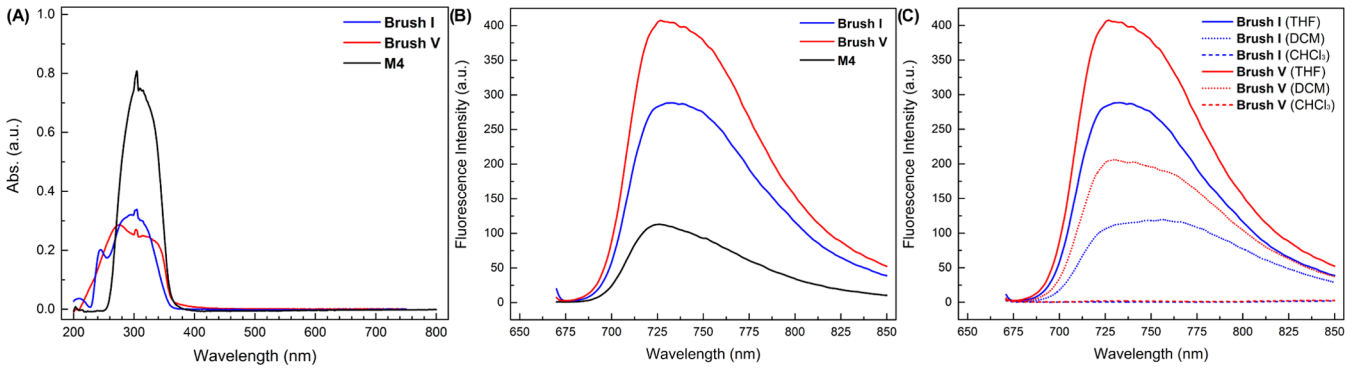

Figure 2. Photophysical properties of polymers bearing pendant TPA functionalities. (A) Representative UV−vis spectra of HTBs and PVTPAs in THF (red, **Brush V**; blue, **Brush I**; black, M4). (B) Fluorescence emission spectra excitation at 658 nm of **Brush V** (red), **Brush I** (blue), and M4 (black) in THF, respectively. (C) Solvent polarity-responsive fluorescence emission spectra of **Brush I** (blue) and **V** (red), respectively. Sample concentrations: 0.1 mg/mL.

Brush II (THF-SEC, Figure S6b) made this additional purification process unattractive. Moreover, thin films prepared from the SEC-purified brushes showed pronounced surface heterogeneities (*vide infra*). Taking account of these facts, we instead purified the HTBs by repeated methanol precipitations and used them in the following studies.

It is noteworthy that the M_n values of purified **Brush I−V** and their precursors (Table S4) from SEC-MALS measurements were less than the theoretical values, calculated from the corresponding ROMP feed ratio and the macromonomer conversions. The discrepancy in molar masses was initially attributed to overestimated specific refractive index increment (dn/dc) values from online SEC measurements. However, the M_n value of **Brush I** derived from the dn/dc value, determined by batch analysis with a differential refractometer, only showed a <10% increase relative to the M_n from online SEC-MALS measurement. This result intrigued us to investigate whether the underestimated M_n values might be related to certain photophysical properties of HTBs in THF solution.

Photophysical Properties of HTBs in Solutions. Figure 2A shows the representative UV−vis absorption spectra of HTBs (**Brush I** and **V**, *ca.* 0.29 and 0.35 mM of TPA concentration, respectively) and the linear NB-PVTPA$_{30}$ (M4, *ca.* 0.34 mM of TPA concentration) in THF. The noticeable variation of absorption intensity between **Brush V** and M4 with comparable TPA concentrations suggested that different stacking modes of TPAs within molecular bottlebrush and linear polymer frameworks could change their photophysical properties. Despite the absence of UV−vis absorption above 400 nm, near-infrared fluorescence emissions with maxima at ∼725 nm were observed for both brushes (Figure 2B) upon excitation at 658 nm, the wavelength for the MALS detector light source. A similar phenomenon was also revealed for the solution of **Brush V** precursor in THF (0.1 mg/mL, ∼0.34 mM of TPA concentration, Figure S7). In comparison with the linear counterpart, the molecular bottlebrush topological factor produced over 2-fold enhancements of the fluorescence emission signals. Due to the partial absorption of the 658 nm irradiated light source, the detector-measured intensities of light scattered by the brushes were subsequently reduced, relative to the linear NB-PVTPA, which resulted in the underestimated molar mass values for bottlebrushes.

The fluorescent properties of HTBs also exhibited a solvent polarity dependence. As shown in Figure 2C, the intensities of 725 nm emissions in less polar dichloromethane (DCM) underwent ∼64 and ∼50% decrease for **Brush I** and **V**, respectively. In chloroform ($CHCl_3$) with the lowest as-surveyed solvent polarity, we did not observe any perceptible near-infrared fluorescence emissions. The perceived solvent polarity responsivity indicated a charge transfer fluorescence character of the brush near-infrared emissions. Comprehensive studies on the mechanism and the structure−activity relationship of these interesting and novel photophysical phenomena are ongoing.

Characterization of HTL Thin Films on Si Wafers. HTL thin films on Si wafers, with film thicknesses commensurate to the contour length of each HTB PNB backbone (Chart S2), were prepared by an optimized spin-casting and thermal annealing protocol. As characterized by tapping-mode atomic force microscopy (AFM) (Figures S8 and S9), the films from **Brush I**, **III**, **IV**, and **V** exhibited homogeneous surface topographies with height root-mean-square roughnesses of <1 nm. The film surface homogeneity was further confirmed by Au_{400}^{4+} cluster secondary-ion mass spectrometry (SIMS, Figure S10 and Table S5), which showed co-emission of PVTPA with PNFHBS from the topmost part of the film in over 79% of the mass spectrometry measurements (see the Supporting Information, SI, for details). For **Brush II** films, obvious defects (depth: ≈5 nm; diameter: >200 nm) were revealed from AFM height imaging, which suggested mixed morphologies of the films.[35] Thin films composed of more ill-defined **Brush II**, obtained from the more extensive $CHCl_3$-SEC purification, were also prepared and imaged by AFM. However, significantly increased defects, in terms of density and feature size, were observed for these films (Figure S11).

From the SIMS fluorine depth profiling of **Brush I**, **III**, and **V** as-cast films (Figure 3A−C; see the SI for details), the F species were predominantly located within the top-7 nm region of each sample, supporting the vertical orientation of brush PNB backbones.[34] These observations indicated that the vertical alignment of HTBs within the films mainly occurred in the solution casting state, driven by the migration of PNFHBS segments to the film−air interface for lowing the surface energy of the film. Upon thermal annealing below the glass transition temperature of HTBs (145 °C, Figure S12), the F^-/C^- side peaks located at *ca.* 15 nm depth of **Brush III** and **V** films decreased, indicating improvement of the brush vertical alignment. For **Brush I** film, the thermal annealing did not result in noticeable enhancement. **Brush III** showed better vertical alignment than **Brush I** and **Brush V**, due to its

https://doi.org/10.1021/jacs.2c00420
J. Am. Chem. Soc. 2022, 144, 8084−8095

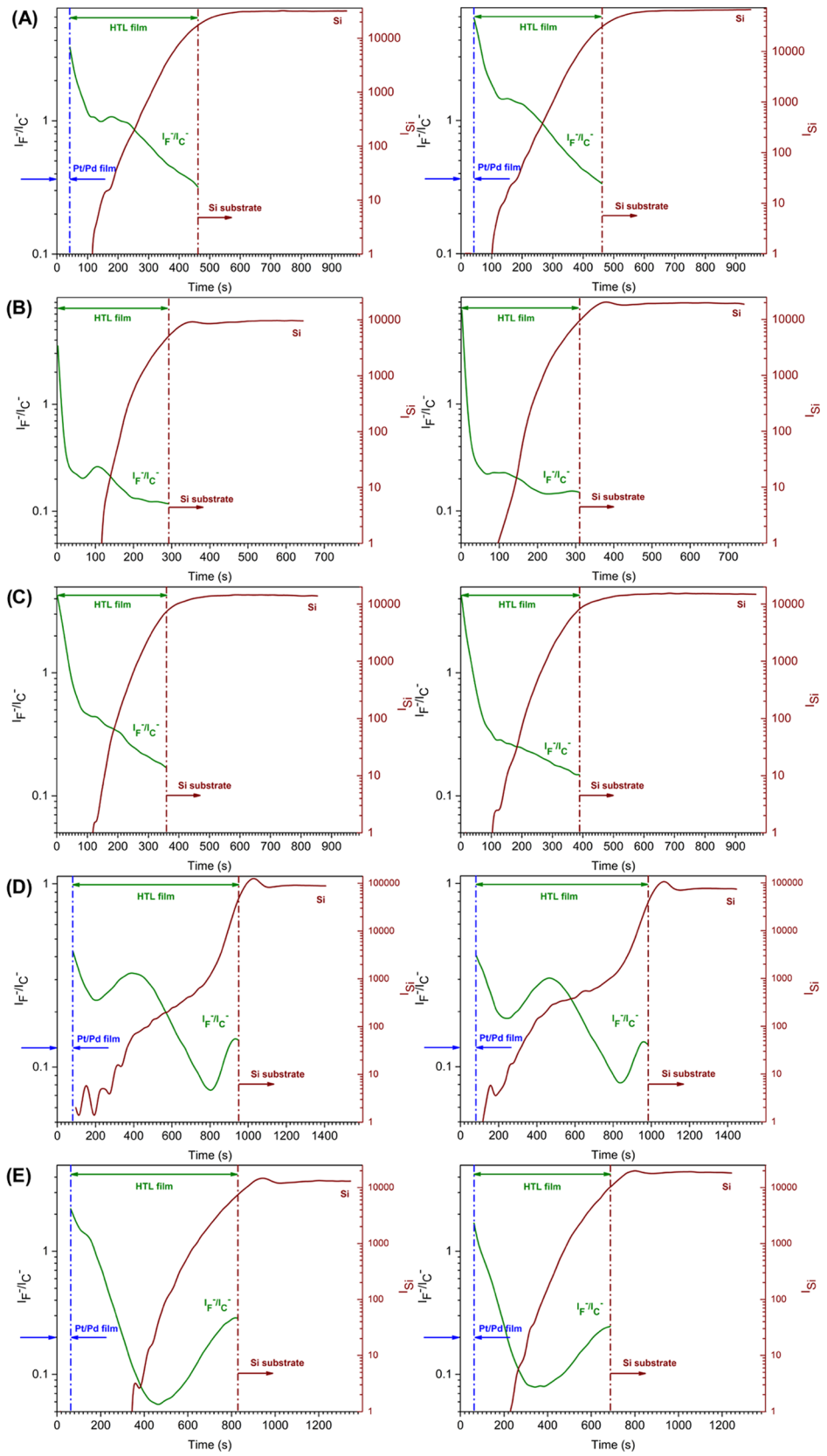

Figure 3. SIMS fluorine depth profiles (left, as-cast; right, thermally annealed) of (A) **Brush I**, (B) **Brush III**, (C) **Brush V**, (D) **Brush II**, and (E) **Brush IV** films on Si wafers, respectively.

structural and compositional characteristics, *i.e.*, relatively stronger substrate adhesion from the longer PVTPA side chains ($PVTPA_{39}$ *vs* $PVTPA_{26}$) and enhanced surface energy-driven assistance from the larger fluorinated blocks ($PNFHBS_{13}$ *vs* $PNFHBS_9$), respectively. The presence of three fluorine-rich domains along the F depth profile of **Brush**

https://doi.org/10.1021/jacs.2c00420
J. Am. Chem. Soc. 2022, 144, 8084−8095

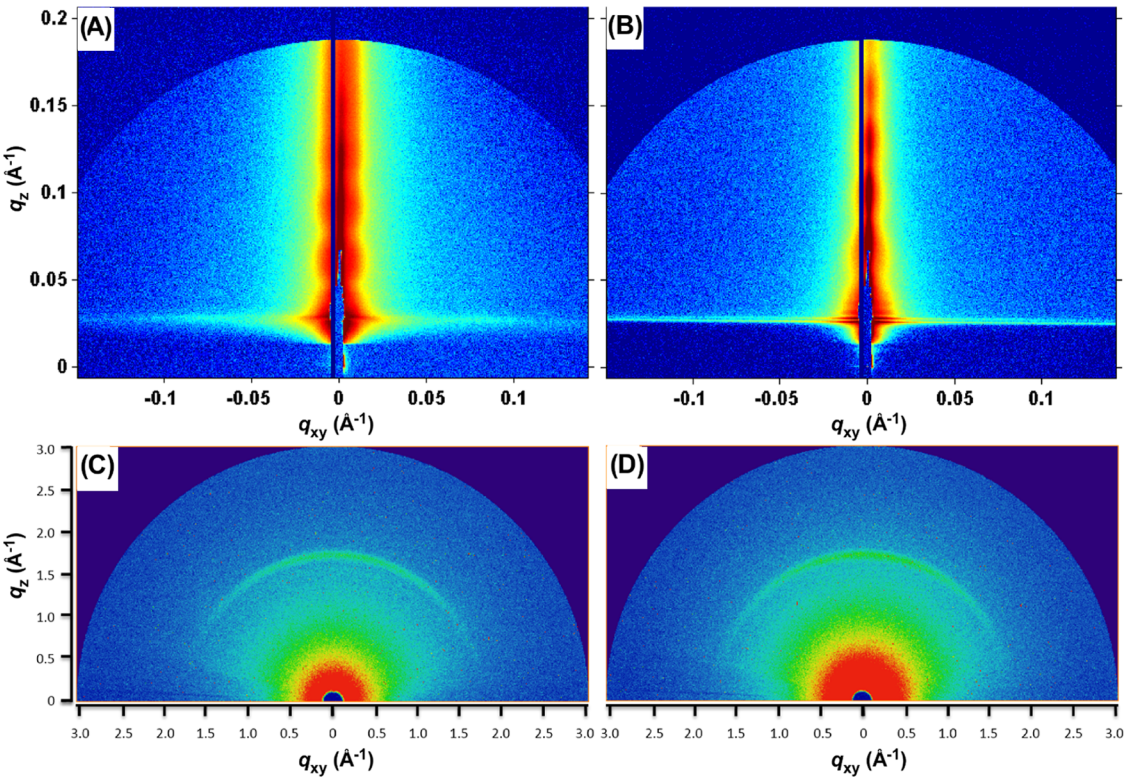

Figure 4. GISAXS (top row) and GIWAXS (bottom row) characterizations of thermally annealed **Brush III** thin films on neat (A, C) and PEDOT:PSS-coated (B, D) Si wafers, respectively; q_{xy} and q_z were defined as coordinates of the reciprocal space.

II films (Figure 3D) indicated that **Brush II** exhibited poor perpendicular substrate alignment. Similar unsatisfactory ordering was observed for **Brush IV** films, which showed an additional F-rich domain near the substrate that did not improve through thermal annealing (Figure 3E). Based on these observations, a DP_n value of 40 might be the threshold for the PNB backbone length of HTBs that could be vertically aligned within a monolayered HTL film.

The molecular orientation of TPAs within HTL films was characterized by variable-angle spectral ellipsometry (VASE, Figure S13).[46] The order parameters (S_{VASE}) were calculated based on eq S1. Briefly, an S_{VASE} value that is closer to −0.5 indicates better anisotropic packing of TPAs within HTL films with π-orbitals that are aligned more parallel to the substrate; see the SI for details) from **Brush I**, **III**, and **V** as-cast films showed preferential "face-on" packing of TPAs with S_{VASE} values of −0.157 ± 0.001, −0.169 ± 0.006, and −0.100 ± 0.006, respectively. After thermal annealing for 3 min, the anisotropy of **Brush III** and **V** films exhibited over 50% improvements (S_{VASE} = −0.302 ± 0.001 and −0.165 ± 0.006, respectively), while the annealed **Brush I** film did not show conspicuous variation (S_{VASE} = −0.152 ± 0.011). Longer thermal annealing times, *i.e.*, 10 min and 20 min, were also attempted. However, the extended annealing time produced a >20% decrease in anisotropy. By comparison, the films from **Brush II** and **IV**, and linear control (NB-PTVPA$_{50}$) polymers showed isotropic packings of TPAs (S_{VASE}s ≈ 0). It should be noted that these S_{VASE} values only represented the spatial orderliness of TPAs within HTL films on neat Si wafers, as VASE was not suitable for anisotropic characterization of multiple-layered films. While typical OLED device contain a HIL, *e.g.*, poly(3,4-ethylenedioxythiophene):polystyrene sulfonate (PEDOT:PSS), under the HTL, the alignment of HTBs in an HTL film could vary, due to additional interactions between PVTPA side chains and a HIL. Therefore, the actual extents of TPA "face-on" packings between **Brush I**, **III**, and **V** in real devices might not be as significant as reflected by these S_{VASE} values.

Brush III HTL Thin Films on PEDOT:PSS HILs. Thermally annealed **Brush III** thin films on substrates coated with PEDOT:PSS HILs were explored. Although the films on both PEDOT:PSS-coated Si wafer and indium tin oxide (ITO) glass exhibited slightly increased heterogeneities (Figures S14a,c *vs* S9c), their Au_{400}^{4+} cluster SIMS surface analyses revealed comparable homogeneities (>85%) and correlation coefficients (∼0.9) as the control film on neat Si wafer. By implementing two-dimensional (2D) grazing-incidence small-angle X-ray scattering (GISAXS),[44] a series of discrete peaks along the out-of-plane direction (q_z) were detected for **Brush III** films on wafer (Figure 4A) and on the HIL-coated Si wafer (Figure 4B), respectively. The absence of scattering patterns along the in-plane (q_{xy}) direction, together with the agreement of film thicknesses by GISAXS, *i.e.*, 21 and 20 nm for films on neat and PEDOT:PSS-coated Si wafers (Figure S15a), respectively, provided additional evidence for the vertical orientation of brush PNB backbones regardless of the types of substrates, although the extent of alignment might have minor differences.

The packing information of TPAs within **Brush III** films on PEDOT:PSS HIL was probed using 2D grazing-incidence wide-angle scattering (GIWAXS).[9,25,47] As shown in Figure 4C,D, there were no noticeable scattering peaks observed along the q_{xy} direction for both films on neat and PEDOT:PSS-coated Si wafers. By comparison, relatively broader $\pi-\pi$ stacking scattering signals along the out-of-plane direction were revealed by GIWAXS. Centered at q_z ∼ 1.845 Å^{-1} (π-

https://doi.org/10.1021/jacs.2c00420
J. Am. Chem. Soc. 2022, 144, 8084−8095

stacking distance, d_π = 3.405 Å) and 1.854 Å^{-1} (d_π = 3.389 Å) for **Brush III** films on Si wafers with and without HIL coating, respectively, the TPA stacking exhibited sufficient similarity (Figure S15b), which confirmed that the preferential "face-on" alignments could be achieved through orthogonal spin-casting of HTBs. Due to the intrinsic crystallinity of ITO, we could not obtain meaningful results from GIWAXS characterization of **Brush III** film on PEDOT:PSS-coated ITO glass (data not shown). Taking account of the ∼40 nm thickness of PEDOT:PSS layer, it is reasonable to speculate that the Si wafer/ITO-induced distinctiveness of HTL films, prepared under same spin-casting and annealing conditions, should be minor.

Electronic Properties of Brush III. The HOMO energy level of **Brush III**, −5.20 eV, was derived from the measured oxidation potential in CH_2Cl_2 by cyclic voltammetry (Figure S16). This value was close to the literature reported HOMO energy level of linear PVTPA (−5.24 eV)[48] and was located within an optimal HTL HOMO energy range (−5.1 to −5.3 eV),[49] which is critical for improving red- and green-phosphorescence OLED device performance.[50] Due to the failure on obtaining the electron affinity by cyclic voltammetry, we did not comprehensively explore the electronic properties of HTBs in solutions.

Hole-Only Device (HOD) Evaluations. Hole-only devices comprising **Brush III** (HOD-**III**), linear NB-PVTPA$_{50}$ (HOD-**LC1**) (Scheme S2), and homobrush P(NB-*g*-PTVPA$_{26}$)$_{30}$ (HOD-**HC1**) as HTLs, respectively, were produced with a configuration of ITO/PEDOT:PSS (40 nm)/HTL (20, 17, and 17 nm by an ellipsometer for HTLs from **Brush III**, NB-PVTPA$_{50}$, and P(NB-*g*-PTVPA$_{26}$)$_{30}$, respectively)/Al (100 nm). The field-dependent space-charge-limited current (SCLC) behavior evaluations[51] revealed that the anisotropic HOD-**III** exhibited two Poole−Frenkel SCLC regimes at 2.0−3.5 and 4.0−5.0 V of applied bias ranges, respectively (Figure 5, red short dash and solid lines through red filled squares, respectively; see the SI for details). The Poole−Frenkel factor (β) of each regime, obtained from the slope of the corresponding linear fitting line, was 0.00579 and 0.00196, respectively. By comparison, the isotropic HOD-**LC1** only showed one Poole−Frenkel SCLC regime in the 4.0−5.0 V range (Figure 5, black solid line through black filled circles) with β of 0.000121. At 5.0 V of driving voltage, the SCLC mobility of HOD-**III** was comparable to that of HOD-**LC1**, *i.e.*, (2.20 ± 0.13) × 10^{-7} *vs* (2.01 ± 0.46) × 10^{-7} cm^2 V^{-1} s^{-1} (calculated based on eq S3 by applying measured currents), although the measured current density was *ca.* 30% lower than the latter (Figure S17a and Table S6). Due to the relatively thinner nature of both HTL films, higher voltages over 5.0 V were not attempted for these devices. For HOD-**HC1**, the HTL with a thickness that was close to the contour length of the P(NB-*g*-PVTPA$_{26}$)$_{30}$ PNB backbone (∼18 nm) showed a small anisotropy (S_{VASE} = −0.043 ± 0.012, Figure S18a), which was attributed to the portions of vertically and obliquely aligned brushes in the film. Two Poole−Frenkel SCLC bias ranges of 2.5−3.5 V (β = 0.00222) and 4.0−5.0 V (β = 0.00133) were identified for HOD-**HC1** (Figure 5, magenta short dash and solid lines through magenta filled triangles, respectively). Herein, the anisotropic packing of TPAs within thin HTLs clearly showed improvement of Poole−Frenkel charge transport at relatively lower driving voltages, which also exhibited good correlation with the extent of "face-on" aligned TPA moieties.

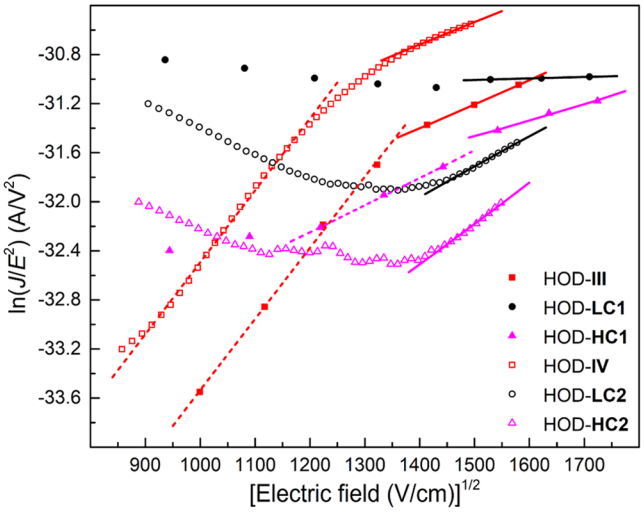

Figure 5. Natural logarithm of J/E^2 *vs* square root of E plots of HODs comprising **Brush III** (HOD-**III**), NB-PVTPA$_{50}$ (HOD-**LC1**), P(NB-*g*-PVTPA$_{26}$)$_{30}$ (HOD-**HC1**), **Brush IV** (HOD-**IV**), PVTPA$_{48}$ (HOD-**LC2**), and P(NB-*g*-PVTPA$_{30}$)$_{35}$ (HOD-**HC2**), respectively. J: current density. E: electric field. The lines were linear fits (R^2 > 0.99) to the space-charge-limited current theory with Poole−Frenkel compensation.

HODs comprising relatively thicker HTLs, *i.e.*, HOD-**IV** from **Brush IV**, HOD-**LC2** from linear PVTPA$_{48}$ (Scheme S2), and HOD-**HC2** from homobrush P(NB-*g*-PVTPA$_{30}$)$_{35}$ with 31, 28, and 29 nm of HTL thickness by ellipsometry, respectively, were then evaluated. The **Brush IV** film on neat Si wafer, prepared under specific protocol (see the SI for details), showed statistically significant S_{VASE} values over the PVTPA$_{48}$ film (−0.045 ± 0.031 *vs* −0.026 ± 0.018, Figure S18b) and the P(NB-*g*-PVTPA$_{30}$)$_{35}$ film (−0.045 ± 0.031 *vs* 0.003 ± 0.006), respectively. Meanwhile, the **Brush IV** film on PEDOT:PSS HIL exhibited sufficient homogeneity (Figure S18c). The SCLC evaluation of HOD-**IV** followed similar trends to HOD-**III** (Figure 5, red unfilled squares *vs* filled squares). Two Poole−Frenkel SCLC regimes at driving voltages of 2.5−4.5 V (β = 0.00586) and 6.0−7.0 V (β = 0.00183), respectively, were identified. Within the 6.0−7.0 V SCLC region of HOD-**LC2** (β = 0.00247) and HOD-**HC2** (β = 0.00332), the current density of HOD-**IV** was over 100% higher than HOD-**LC2** and HOD-**HC2** at 6.0, 6.5, and 7.0 V, respectively (Figure S17a and Table S6). These HOD studies allowed for observations of regions of SCLC, as evidenced by linearity in the Poole−Frenkel plots (Figure 5), and revealed stark differences between the bottlebrush and liner control polymer topologies, as an initial evaluation prior to fabrication and testing of performance in full OLED device configurations.

OLED Full Device Evaluations. Stacked thermally activated delayed fluorescence (TADF) OLED[52−56] full devices comprising sequential layers for the operations of hole injection, hole transport, emission, and electron transport successively built up from the anode to the cathode were prepared and utilized to explore the relationship between device performance and the anisotropy of HTL. **Brush I**, **III**, and **V**, PVTPA$_{48}$, and P(NB-*g*-PVTPA$_{30}$)$_{35}$ were employed as the HTLs (Figure S19). Another linear polymer control with intrinsically high hole mobility, poly(9,9-dioctylfluorene-*alt*-*N*-(4-*sec*-butylphenyl)-diphenylamine) (TFB), was also introduced and compared. Upon fabricating brushes, or PVTPA$_{48}$,

https://doi.org/10.1021/jacs.2c00420
J. Am. Chem. Soc. 2022, 144, 8084−8095

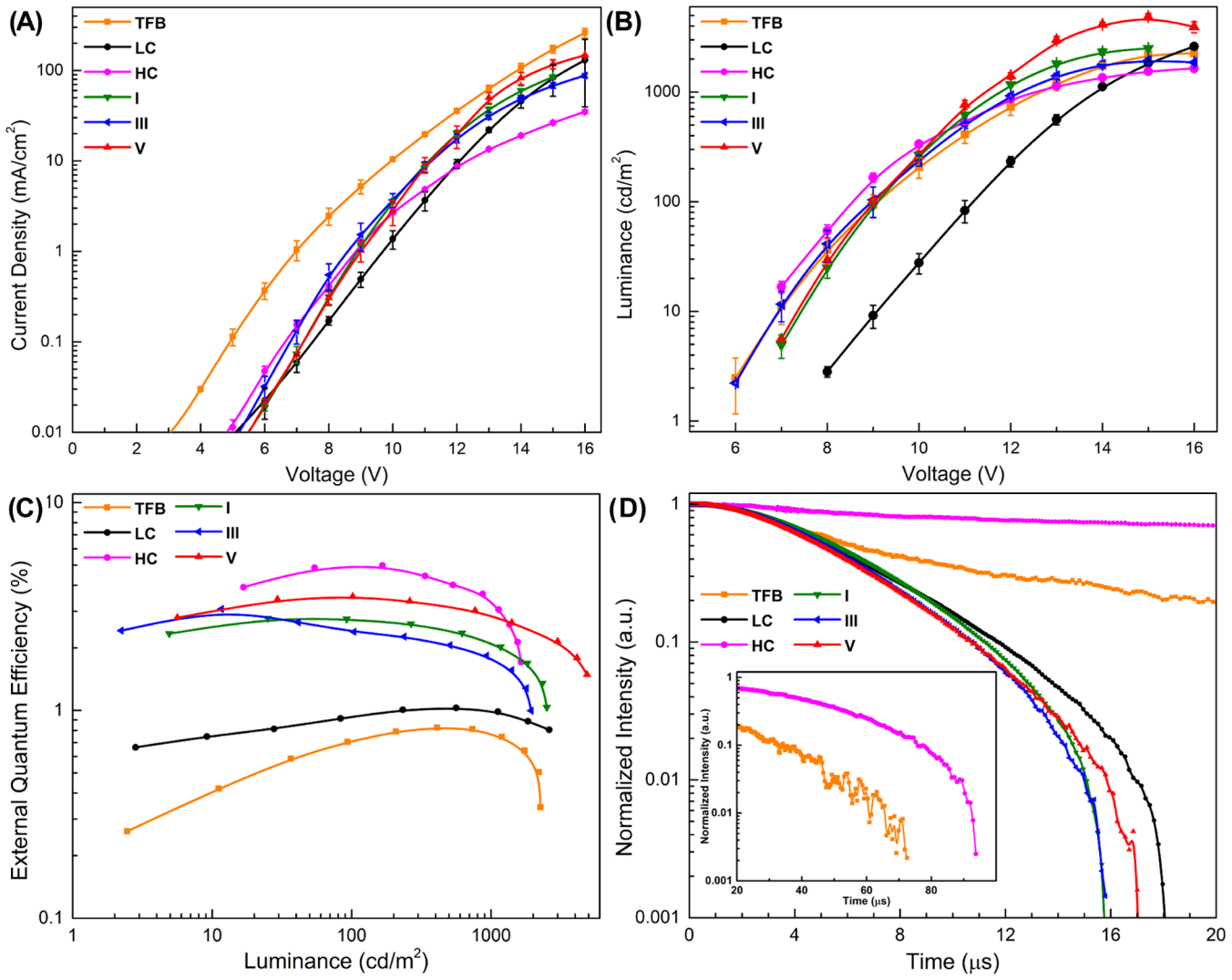

Figure 6. Performance evaluations of green OLED full devices comprising **Brush I**, **III**, and **V**, $PVTPA_{48}$, $P(NB\text{-}g\text{-}PVTPA_{30})_{35}$, and TFB, respectively, as HTLs. (A, B) Current density (A) and luminance (B) *vs* voltage plots, respectively. (C) External quantum efficiency *vs* luminance plots. (D) Transient electroluminescence profiles of devices tested at 295 K and 10 V for a 1000 μs pulse; the inset shows the decay profiles of devices **TFB** and **HC** after 20 μs.

or TFB on PEDOS:PSS-coated ITO glass through spin-casting and thermal annealing, 9,10-bis(4-(9*H*-carbazol-9-yl)-2,6-dimethylphenyl)-9,10-diboraanthracene (CzDBA, a green TADF emitter),[57] 1,3,5-tri(3-pyridyl)-phen-3-ylbenzene (TmPyPB), 8-hydroxyquinolatolithium (Liq), and Al were sequentially deposited through vacuum depositions to construct emissive layer, ETL, electron injection layer, and cathode, respectively (Figure S19). All **I**, **III**, **V**, **LC**, **HC**, and **TFB** devices were built up based on the following configuration: ITO/PEDOT:PSS (40 nm)/HTL (~25 nm)/CzDBA (40 nm)/TmPyPB (45 nm)/Liq (1 nm)/Al (100 nm). For each device, three randomly selected pixels were measured (Figures S20−S25).

The electroluminescence spectra of all TADF-OLED devices showed yellow-green emissions with peaks of maximum intensity in the range of 558−574 nm (Figure S26a), which ensured direct comparisons between device performances. Our hole mobility testing on linear PVTPAs, homobrushes, and **Brush III** and **IV**, as well as literature reports,[48,58] indicated that the polyvinyl polymers bearing pendant TPA functionalities, particularly in HTLs with thickness < 50 nm, could not provide hole mobility over 2×10^{-5} cm^2 V^{-1} s^{-1}, which was at least 2 orders of magnitude lower than TFB (2×10^{-3} cm^2 V^{-1} s^{-1}). Therefore, the current densities of devices **I**, **III**, **V**, **LC**, and **HC** were consistently lower than device **TFB** within the whole range of bias, regardless of the TPA packing mode variations within HTLs (Figure 6A). The threshold voltages, at a current density of 0.01 mA/cm^2, of devices **I**, **III**, **V**, **LC**, and **HC** were also ~2 V higher than that of the **TFB** device.

However, the luminance of devices did not follow the observed current density trend. Starting from 6 V, which produced meaningful luminance (≥2 cd/m^2), device **III** with the highest anisotropic packing of TPAs exhibited comparable luminance to device **TFB** (Figure 6B, blue *vs* orange profile), in spite of the obvious difference between intrinsic hole mobilities. As a note, compared with the device **TFB**, device **III** was more "sensitive" at a high current density (Figure S26b) due to complicated annihilation mechanisms.[59] For devices **I** and **V** with relatively lower extents of anisotropic TPA packings than **III**, their luminance performance at driving voltage ranged from 6 to 8 V (Figure 6B, olive and red profiles for **I** and **V**, respectively) were subsidiary than **III** and **TFB**. However, upon applying bias exceeding 10 V, **I** and **V**

https://doi.org/10.1021/jacs.2c00420
J. Am. Chem. Soc. 2022, 144, 8084−8095

produced higher luminance than both **III** and **TFB**. Particularly, device **V** built up from **Brush V** with the largest amount of TPA charge carriers per polymer achieved the highest maximum luminance of 4880 cd/m^2 (Table S7), which was ∼95, ∼150, and ∼110% enhancement compared with **I**, **III**, and **TFB**, respectively. In contrast, device **LC** with isotropic HTL continuously showed the lowest luminance at each driving voltage until 15 V (Figure 6B, black profile). Herein, anisotropic packing of TPAs within HTLs of green TADF-OLEDs revealed superiority on improving device performance. The relatively higher extent of TPA "face-on" packing in device **III** afforded better luminance at relatively lower driving voltages (6−8 V), while device **V**, with moderate HTL anisotropy but bearing more TPA functionalities, covered the 11−15 V bias "window" and provided the largest maximum luminance at 15 V.

Interestingly, device **HC** also showed significantly improved luminance performance over device **LC** at each of the surveyed bias lower than 14 V (Figure 6B, magenta *vs* black profile), although the ∼25 nm P(NB-*g*-PVTPA$_{30}$)$_{35}$ HTL only exhibited marginally anisotropic packing of TPAs (S_{VASE} = −0.030 ± 0.002) over the ∼25 nm PVTPA$_{48}$ HTL (S_{VASE} = −0.009 ± 0.006). The luminance of **HC** at relatively lower driving voltages (6−10 V) were over 10-fold higher than **LC** and were comparable to **III**, which suggested that the high content of HT moieties and the absence of fluorocarbon insulators between HTL and emissive layer interface might compensate the lower HTL anisotropy within this bias range. Starting from 11 V, device **HC** exhibited the lowest current densities among the devices built up from HT polymers with bottlebrush topology (devices **HC**, **I**, **III**, and **V**, Figure 6A, magenta *vs* olive, blue, and red profiles). These results indicated that the introduction of a single bottlebrush topological factor without thoroughly anisotropic packing of TPAs in an HTL could not enable high current density. Therefore, the luminance of device **HC** was over 100% lower than device **V** within the bias range of 13−16 V (Figure 6B, magenta *vs* red profile).

As shown in Figure 6C, the external quantum efficiencies (EQEs) of devices **I**, **III**, and **V** from corresponding HTBs exhibited significant enhancements over devices **LC** and **TFB** built up from linear polymers at a luminance less than 1000 cd/m^2. The EQE maxima of devices **I**, **III**, and **V** were 2.8, 3.1, and 3.5%, respectively, which were at least 1.8-fold higher than device **LC** (1.0%) and over 2.5-fold higher than device **TFB** (0.8%). Even at a current density of 30 mA/cm^2 (Figure S26b), devices **I**, **III**, and **V** still maintained over 50% enhanced EQEs than devices **LC** and **TFB** (EQE ≈ 1.0 and 0.7% for **LC** and **TFB**, respectively) at the same current density. Similar tendencies were observed for the device current and power efficiencies (Figure S26c,d, respectively). Surprisingly, **HC** exhibited the highest maximum external quantum, current, and power efficiency values (Table S7) among all OLED devices, which further supported the role of bottlebrush topology in improving the device efficiency. However, the lack of TPA anisotropy in the HTL of **HC** caused 34% EQE roll-off at a luminance of 1000 cd/m^2 (Table S7), which was more significant in comparison with **I** and **V** (25 and 20% roll-off values for **I** and **V**, respectively). It is noteworthy that the maximum luminance and efficiencies of the device consisting **Brush V** as an HTL were inferior to the state-of-the-art CzDBA-based green fully evaporated TADF-OLED with optimized energy-level alignment and host-dopant emissive layer.[57] These established tactics will be incorporated in our future design and investigation of HTBs for solution-processable anisotropic HTLs that can realize high electroluminescence performance of the optimal OLED architectures.

Unlike device **TFB**, which exhibited a long transient electroluminescence tail, accounting for low luminance, low efficiency and significant efficiency roll offs (Figure 6D), the devices with **Brush I**, **III**, and **V** showed faster radiative decay and thus reduced annihilation processes compared to device **LC** with linear PVTPA$_{48}$. This observation was attributed to efficient charge carrier injection and reduced exciton quenching, which is the superiority of the anisotropic HTLs. In addition, it helps to make the device run and response much faster for the cutting-edge active matrix displays. By sharp comparison, the decay time of device **HC** was over 400% longer than **I**, **III**, and **V**, which further elucidated the advantage of highly anisotropic "face-on" packing of TPAs within an HTL.

Based on the results from OLEDs, it could be summarized that the anisotropic HTL (S_{VASE} ≈ −0.17) built up from **Brush V**, *i.e.*, P(NB-*g*-(PVTPA$_{22}$-*b*-PNFHB$_9$))$_{10}$-*b*-P(NB-*g*-PVTPA$_{39}$)$_{30}$, enabled the superior performances, including the high maximum luminance, good efficiency, and small efficiency roll-off, and short transient electroluminescent decay. Therefore, the structural characteristics of **Brush V**, such as the PNB backbone DP value, high content of HT moieties, appropriate F content, and concentric and lengthwise block ratios, might be adopted as foundational parameters for developing anisotropic HTBs with inherently high hole mobilities toward achieving advanced HTLs that can further improve charge balance inside the emissive layer.

CONCLUSIONS

In conclusion, P(NB-*g*-(PVTPA-*b*-PNFHB))-*b*-P(NB-*g*-PVTPA) bottlebrush polymers with precisely controllable compositions and dimensions were synthesized by ROMP of well-defined macromonomers. The resulting HTBs could be vertically aligned on substrates through the use of surface-directing fluorinated moieties to afford monolayered HTL thin films. The vertical alignment of brush backbone assisted the preferential "face-on" molecular orientations of TPA units, demonstrated by the high-order parameter from VASE quantifications. Green TADF-OLED device comprising HTBs as anisotropic HTLs indicated significant improvements in electroluminescence performance, in comparison with the isotropic counterpart. Although the intrinsic hole mobilities of HTB-based HTLs was at least 3 orders of magnitude lower than the TFB-based control, the higher extent of TPA anisotropic packing could be beneficial to compensate the charge imbalance in the device, which resulted in comparable luminance and over 2-fold of efficiency enhancements, respectively. Our contemporary approach relying upon chemistry toolbox revealed promising potentials for resolving the long-lasting obstacle in optoelectronics. It is also expected that this platform could be extended to vertically alignable multiblock structures[60] capable of multiple tasks of ETL, emissive layer, and HTL through a single-stage fabrication for the construction of multiple-layered OLEDs.

ASSOCIATED CONTENT

Supporting Information

The Supporting Information is available free of charge at https://pubs.acs.org/doi/10.1021/jacs.2c00420.

https://doi.org/10.1021/jacs.2c00420
J. Am. Chem. Soc. 2022, 144, 8084−8095

Experimental details for the preparation and characterization of polymers, films, and devices, and additional data (PDF)

AUTHOR INFORMATION

Corresponding Authors

Guorong Sun − *Department of Chemistry, Texas A&M University, College Station, Texas 77842, United States*; Email: guorong.sun@chem.tamu.edu

Guohua Xie − *Sauvage Center for Molecular Sciences and Hubei Key Lab on Organic and Polymeric Optoelectronic Materials, Department of Chemistry, Wuhan University, Wuhan 430072, China*; orcid.org/0000-0003-0764-7889; Email: guohua.xie@whu.edu.cn

Peter Trefonas − *DuPont, Electronics and Imaging Division, Marlborough, Massachusetts 01752, United States*; Email: p3voices@gmail.com

Karen L. Wooley − *Department of Chemistry, Department of Materials Science and Engineering, and Department of Chemical Engineering, Texas A&M University, College Station, Texas 77842, United States*; orcid.org/0000-0003-4086-384X; Email: wooley@chem.tamu.edu

Authors

Nari Kang − *Department of Chemistry and Department of Materials Science and Engineering, Texas A&M University, College Station, Texas 77842, United States;* Present Address: Tapeout Technology Development, Intel Corporation, Hillsboro, Oregon 97124, United States

Sangho Cho − *Department of Chemistry, Texas A&M University, College Station, Texas 77842, United States;* Present Address: Materials Architecturing Research Center, Korea Institute of Science and Technology (KIST) and Division of Nano & Information Technology, KIST School, Korea University of Science and Technology, Seoul 02792, Republic of Korea.; orcid.org/0000-0002-9627-5310

Eric E. Leonhardt − *Department of Chemistry, Texas A&M University, College Station, Texas 77842, United States;* Present Address: Sullivan Park Science & Technology Center, Corning Research & Development Corporation, Painted Post, New York 14870, United States.

Chun Liu − *The Dow Chemical Company, Midland, Michigan 48667, United States*

Stanislav V. Verkhoturov − *Department of Chemistry, Texas A&M University, College Station, Texas 77842, United States*

William Henry Hunter Woodward − *The Dow Chemical Company, Midland, Michigan 48667, United States;* orcid.org/0000-0002-5814-3237

Michael J. Eller − *Department of Chemistry, Texas A&M University, College Station, Texas 77842, United States;* Present Address: Department of Chemistry and Biochemistry, California State University, Northridge, Northridge, California 91330, United States.; orcid.org/0000-0002-9069-2180

Tianyu Yuan − *Department of Chemistry, Texas A&M University, College Station, Texas 77842, United States;* orcid.org/0000-0002-6698-5178

Thomas C. Fitzgibbons − *The Dow Chemical Company, Lake Jackson, Texas 77566, United States*

Yannick P. Borguet − *Department of Chemistry, Texas A&M University, College Station, Texas 77842, United States*

Ashlee A. Jahnke − *Department of Chemistry, Texas A&M University, College Station, Texas 77842, United States*

Anatoliy N. Sokolov − *The Dow Chemical Company, Midland, Michigan 48667, United States*

Travis McIntire − *The Dow Chemical Company, Midland, Michigan 48667, United States*

Carl Reinhardt − *The Dow Chemical Company, Midland, Michigan 48667, United States*

Lei Fang − *Department of Chemistry, Texas A&M University, College Station, Texas 77842, United States*; orcid.org/0000-0003-4757-5664

Emile A. Schweikert − *Department of Chemistry, Texas A&M University, College Station, Texas 77842, United States*; orcid.org/0000-0003-3964-7998

Liam Patrick Spencer − *The Dow Chemical Company, Lake Jackson, Texas 77566, United States*

Complete contact information is available at: https://pubs.acs.org/10.1021/jacs.2c00420

Author Contributions

⋈N.K., S.C., and E.E.L. contributed equally.

Notes

The authors declare no competing financial interest.

ACKNOWLEDGMENTS

The authors thank Dow Chemical Company and DuPont (collaborative research agreements), the National Science Foundation (DMR-1507429 and DMR-1905818), and the Welch Foundation (W. T. Doherty-Welch Chair, A-0001; Welch Research Grant, A-1898) for support. E.E.L. was supported by the National Aeronautics and Space Administration (NASA) through the NASA Space Technology Research Fellowship (NSTRF) program, Grant No. NNX15AQ08H. Dr. Fan Yang is acknowledged for cluster SIMS, Dr. Yen-Hao Lin for GISAXS, Dr. Yang Zou for CV measurements, Dr. Mingqi Li (DuPont) for helpful discussions, and Rui Wang for help with illustrations. Portions of this work were performed at the DuPont-Northwestern-Dow Collaborative Access Team (DND-CAT) located at Sector 5 of the Advanced Photon Source (APS). DND-CAT was supported by Northwestern University, E.I. DuPont de Nemours & CO., and The Dow Chemical Company. The research used resources at the Advanced Photon Source, a U.S. Department of Energy (DOE) Office of Science User Facility operated for the DOE Office of Science by Argonne National Laboratory under Contract No. DE-AC02-06CH11357.

REFERENCES

(1) Yokoyama, D. Molecular Orientation in Small-Molecule Organic Light-Emitting Diodes. *J. Mater. Chem.* **2011**, *21*, 19187−19202.

(2) Schmidt, T. D.; Lampe, T.; Sylvinson, M. R. D.; Djurovich, P. I.; Thompson, M. E.; Brütting, W. Emitter Orientation as a Key Parameter in Organic Light-Emitting Diodes. *Phys. Rev. Appl.* **2017**, *8*, No. 037001.

(3) Kim, K.-H.; Kim, J.-J. Origin and Control of Orientation of Phosphorescent and TADF Dyes for High-Efficiency OLEDs. *Adv. Mater.* **2018**, *30*, No. 1705600.

(4) Salehi, A.; Fu, X.; Shin, D.-H.; So, F. Recent Advances in OLED Optical Design. *Adv. Funct. Mater.* **2019**, *29*, No. 1808803.

(5) Watanabe, Y.; Sasabe, H.; Kido, J. Review of Molecular Engineering for Horizontal Molecular Orientation in Organic Light-Emitting Devices. *Bull. Chem. Soc. Jpn.* **2019**, *92*, 716−728.

(6) Yokoyama, D.; Sakaguchi, A.; Suzuki, M.; Adachi, C. Horizontal Molecular Orientation in Vacuum-Deposited Organic Amorphous Films of Hole and Electron Transport Materials. *Appl. Phys. Lett.* **2008**, *93*, No. 173302.
(7) Kim, J. Y.; Yokoyama, D.; Adachi, C. Horizontal Orientation of Disk-like Hole Transport Molecules and Their Application for Organic Light-Emitting Diodes Requiring a Lower Driving Voltage. *J. Phys. Chem. C* **2012**, *116*, 8699−8706.
(8) Kim, J. Y.; Yasuda, T.; Yang, Y. S.; Adachi, C. Bifunctional Star-Burst Amorphous Molecular Materials for OLEDs: Achieving Highly Efficient Solid-State Luminescence and Carrier Transport Induced by Spontaneous Molecular Orientation. *Adv. Mater.* **2013**, *25*, 2666−2671.
(9) Wakamiya, A.; Nishimura, H.; Fukushima, T.; Suzuki, F.; Saeki, A.; Seki, S.; Osaka, I.; Sasamori, T.; Murata, M.; Murata, Y.; Kaji, H. On-Top π-Stacking of Quasiplanar Molecules in Hole-Transporting Materials: Inducing Anisotropic Carrier Mobility in Amorphous Films. *Angew. Chem., Int. Ed.* **2014**, *53*, 5800−5804.
(10) Wu, C.-C.; Liu, T.-L.; Hung, W.-Y.; Lin, Y.-T.; Wong, K.-T.; Chen, R.-T.; Chen, Y.-M.; Chien, Y.-Y. Unusual Nondispersive Ambipolar Carrier Transport and High Electron Mobility in Amorphous Ter(9,9-diarylfluorene)s. *J. Am. Chem. Soc.* **2003**, *125*, 3710−3711.
(11) Yokoyama, D.; Sakaguchi, A.; Suzuki, M.; Adachi, C. Enhancement of Electron Transport by Horizontal Molecular Orientation of Oxadiazole Planar Molecules in Organic Amorphous Films. *Appl. Phys. Lett.* **2009**, *95*, No. 243303.
(12) Watanabe, Y.; Sasabe, H.; Yokoyama, D.; Beppu, T.; Katagiri, H.; Pu, Y.-J.; Kido, J. Simultaneous Manipulation of Intramolecular and Intermolecular Hydrogen Bonds in n-Type Organic Semiconductor Layers: Realization of Horizontal Orientation in OLEDs. *Adv. Opt. Mater.* **2015**, *3*, 769−773.
(13) Ediger, M. D.; de Pablo, J.; Yu, L. Anisotropic Vapor-Deposited Glasses: Hybrid Organic Solids. *Acc. Chem. Res.* **2019**, *52*, 407−414.
(14) Kulkarni, A. P.; Tonzola, C. J.; Babel, A.; Jenekhe, S. A. Electron Transport Materials for Organic Light-Emitting Diodes. *Chem. Mater.* **2004**, *16*, 4556−4573.
(15) Huang, F.; Cheng, Y.-J.; Zhang, Y.; Liu, M. S.; Jen, A. K. Y. Crosslinkable Hole-Transporting Materials for Solution Processed Polymer Light-Emitting Diodes. *J. Mater. Chem.* **2008**, *18*, 4495−4509.
(16) Xiao, L.; Chen, Z.; Qu, B.; Luo, J.; Kong, S.; Gong, Q.; Kido, J. Recent Progresses on Materials for Electrophosphorescent Organic Light-Emitting Devices. *Adv. Mater.* **2011**, *23*, 926−952.
(17) Beaujuge, P. M.; Fréchet, J. M. J. Molecular Design and Ordering Effects in π-Functional Materials for Transistor and Solar Cell Applications. *J. Am. Chem. Soc.* **2011**, *133*, 20009−20029.
(18) Yen, H.-J.; Liou, G.-S. Design and Preparation of Triphenylamine-based Polymeric Materials towards Emergent Optoelectronic Applications. *Prog. Polym. Sci.* **2019**, *89*, 250−287.
(19) Chen, M. S.; Lee, O. P.; Niskala, J. R.; Yiu, A. T.; Tassone, C. J.; Schmidt, K.; Beaujuge, P. M.; Onishi, S. S.; Toney, M. F.; Zettl, A.; Fréchet, J. M. J. Enhanced Solid-State Order and Field-Effect Hole Mobility through Control of Nanoscale Polymer Aggregation. *J. Am. Chem. Soc.* **2013**, *135*, 19229−19236.
(20) Noriega, R.; Rivnay, J.; Vandewal, K.; Koch, F. P. V.; Stingelin, N.; Smith, P.; Toney, M. F.; Salleo, A. A General Relationship between Disorder, Aggregation and Charge Transport in Conjugated Polymers. *Nat. Mater.* **2013**, *12*, 1038−1044.
(21) Jeong, C. H.; Godumala, M.; Yoon, J.; Choi, S.; Kim, Y. W.; Choi, D. H.; Cho, M. J.; Choi, D. H. Hole-Transporting Side-Chain Polymer Bearing a Thermally Crosslinkable Bicyclo[4.2.0]octa-1,3,5-trien-3-yl Group for High-Performing Thermally Activated Delayed Fluorescence OLED. *ACS Appl. Mater. Interfaces* **2019**, *11*, 17602−17609.
(22) Lee, J. H.; Jeong, C. H.; Godumala, M.; Kim, C. Y.; Kim, H. J.; Hwang, J. H.; Kim, Y. W.; Choi, D. H.; Cho, M. J.; Choi, D. H. Rational Design, Synthesis, and Characterization of a Photocrosslinkable Hole-Transporting Polymer for High Performance Solution-Processed Thermally Activated Delayed Fluorescence OLEDs. *J. Mater. Chem. C* **2020**, *8*, 4572−4579.
(23) Sun, W.; Xie, L.; Guo, X.; Su, W.; Zhang, Q. Photocross-Linkable Hole Transport Materials for Inkjet-Printed High-Efficient Quantum Dot Light-Emitting Diodes. *ACS Appl. Mater. Interfaces* **2020**, *12*, 58369−58377.
(24) Lee, J. H.; Hwang, J.; Kim, C. W.; Harit, A. K.; Woo, H. Y.; Kim, H. J.; Kim, Y. W.; Choi, D. H.; Cho, M. J.; Choi, D. H. New Hole Transport Styrene Polymers Bearing Highly π-Extended Conjugated Side-Chain Moieties for High-Performance Solution-Processable Thermally Activated Delayed Fluorescence OLEDs. *Polym. Chem.* **2021**, *12*, 1692−1699.
(25) Xing, X.; Zhong, L.; Zhang, L.; Chen, Z.; Qu, B.; Chen, E.; Xiao, L.; Gong, Q. Essential Differences of Organic Films at the Molecular Level via Vacuum Deposition and Solution Processes for Organic Light-Emitting Diodes. *J. Phys. Chem. C* **2013**, *117*, 25405−25408.
(26) Verduzco, R.; Li, X.; Pesek, S. L.; Stein, G. E. Structure, Function, Self-Assembly, and Applications of Bottlebrush Copolymers. *Chem. Soc. Rev.* **2015**, *44*, 2405−2420.
(27) Müllner, M.; Müller, A. H. E. Cylindrical Polymer Brushes−Anisotropic Building Blocks, Unimolecular Templates and Particulate Nanocarriers. *Polymer* **2016**, *98*, 389−401.
(28) Xie, G.; Martinez, M. R.; Olszewski, M.; Sheiko, S. S.; Matyjaszewski, K. Molecular Bottlebrushes as Novel Materials. *Biomacromolecules* **2019**, *20*, 27−54.
(29) Kawamoto, K.; Zhong, M.; Gadelrab, K. R.; Cheng, L.-C.; Ross, C. A.; Alexander-Katz, A.; Johnson, J. A. Graft-through Synthesis and Assembly of Janus Bottlebrush Polymers from A-Branch-B Diblock Macromonomers. *J. Am. Chem. Soc.* **2016**, *138*, 11501−11504.
(30) Guo, Z.-H.; Le, A. N.; Feng, X.; Choo, Y.; Liu, B.; Wang, D.; Wan, Z.; Gu, Y.; Zhao, J.; Li, V.; Osuji, C. O.; Johnson, J. A.; Zhong, M. Janus Graft Block Copolymers: Design of a Polymer Architecture for Independently Tuned Nanostructures and Polymer Properties. *Angew. Chem., Int. Ed.* **2018**, *57*, 8493−8497.
(31) Sauvé, E. R.; Tonge, C. M.; Hudson, Z. M. Aggregation-Induced Energy Transfer in Color-Tunable Multiblock Bottlebrush Nanofibers. *J. Am. Chem. Soc.* **2019**, *141*, 16422−16431.
(32) Boyle, B. M.; Collins, J. L.; Mensch, T. E.; Ryan, M. D.; Newell, B. S.; Miyake, G. M. Impact of Backbone Composition on Homopolymer Dynamics and Brush Block Copolymer Self-Assembly. *Polym. Chem.* **2020**, *11*, 7147−7158.
(33) He, Q.; Ku, K. H.; Vijayamohanan, H.; Kim, B. J.; Swager, T. M. Switchable Full-Color Reflective Photonic Ellipsoidal Particles. *J. Am. Chem. Soc.* **2020**, *142*, 10424−10430.
(34) Sun, G.; Cho, S.; Clark, C.; Verkhoturov, S. V.; Eller, M. J.; Li, A.; Pavía-Jimenez, A.; Schweikert, E. A.; Thackeray, J. W.; Trefonas, P.; Wooley, K. L. Nanoscopic Cylindrical Dual Concentric and Lengthwise Block Brush Terpolymers as Covalent Preassembled High-Resolution and High-Sensitivity Negative-Tone Photoresist Materials. *J. Am. Chem. Soc.* **2013**, *135*, 4203−4206.
(35) Sun, G.; Cho, S.; Yang, F.; He, X.; Pavía-Sanders, A.; Clark, C.; Raymond, J. E.; Verkhoturov, S. V.; Schweikert, E. A.; Thackeray, J. W.; Trefonas, P.; Wooley, K. L. Advanced Photoresist Technologies by Intricate Molecular Brush Architectures: Diblock Brush Terpolymer-Based Positive-Tone Photoresist Materials. *J. Polym. Sci., Part A: Polym. Chem.* **2015**, *53*, 193−199.
(36) Banquy, X.; Burdyńska, J.; Lee, D. W.; Matyjaszewski, K.; Israelachvili, J. Bioinspired Bottle-Brush Polymer Exhibits Low Friction and Amontons-like Behavior. *J. Am. Chem. Soc.* **2014**, *136*, 6199−6202.
(37) Adibnia, V.; Olszewski, M.; De Crescenzo, G.; Matyjaszewski, K.; Banquy, X. Superlubricity of Zwitterionic Bottlebrush Polymers in the Presence of Multivalent Ions. *J. Am. Chem. Soc.* **2020**, *142*, 14843−14847.
(38) Jia, F.; Lu, X.; Wang, D.; Cao, X.; Tan, X.; Lu, H.; Zhang, K. Depth-Profiling the Nuclease Stability and the Gene Silencing Efficacy of Brush-Architectured Poly(ethylene glycol)−DNA Conjugates. *J. Am. Chem. Soc.* **2017**, *139*, 10605−10608.

https://doi.org/10.1021/jacs.2c00420
J. Am. Chem. Soc. 2022, 144, 8084−8095

(39) Vohidov, F.; Andersen, J. N.; Economides, K. D.; Shipitsin, M. V.; Burenkova, O.; Ackley, J. C.; Vangamudi, B.; Nguyen, H. V. T.; Gallagher, N. M.; Shieh, P.; Golder, M. R.; Liu, J.; Dahlberg, W. K.; Ehrlich, D. J. C.; Kim, J.; Kristufek, S. L.; Huh, S. J.; Neenan, A. M.; Baddour, J.; Paramasivan, S.; de Stanchina, E.; KC, G.; Turnquist, D. J.; Saucier-Sawyer, J. K.; Kopesky, P. W.; Brady, S. W.; Jessel, M. J.; Reiter, L. A.; Chickering, D. E.; Johnson, J. A.; Blume-Jensen, P. Design of BET Inhibitor Bottlebrush Prodrugs with Superior Efficacy and Devoid of Systemic Toxicities. *J. Am. Chem. Soc.* **2021**, *143*, 4714−4724.
(40) Boyle, B. M.; Heinz, O.; Miyake, G. M.; Ding, Y. Impact of the Pendant Group on the Chain Conformation and Bulk Properties of Norbornene Imide-Based Polymers. *Macromolecules* **2019**, *52*, 3426−3434.
(41) Chan, J. M.; Kordon, A. C.; Zhang, R.; Wang, M. Direct Visualization of Bottlebrush Polymer Conformations in the Solid State. *Proc. Natl. Acad. Sci. U.S.A.* **2021**, *118*, No. e2109534118.
(42) Crossland, E. J. W.; Cunha, P.; Scroggins, S.; Moratti, S.; Yurchenko, O.; Steiner, U.; Hillmyer, M. A.; Ludwigs, S. Soft-Etch Mesoporous Hole-Conducting Block Copolymer Templates. *ACS Nano* **2010**, *4*, 962−966.
(43) Williams, P. E.; Moughton, A. O.; Patterson, J. P.; Khodabakhsh, S.; O'Reilly, R. K. Exploring RAFT Polymerization for the Synthesis of Bipolar Diblock Copolymers and Their Supramolecular Self-Assembly. *Polym. Chem.* **2011**, *2*, 720−729.
(44) Brendel, J. C.; Liu, F.; Lang, A. S.; Russell, T. P.; Thelakkat, M. Macroscopic Vertical Alignment of Nanodomains in Thin Films of Semiconductor Amphiphilic Block Copolymers. *ACS Nano* **2013**, *7*, 6069−6078.
(45) Chong, Y. K.; Moad, G.; Rizzardo, E.; Thang, S. H. Thiocarbonylthio End Group Removal from RAFT-Synthesized Polymers by Radical-Induced Reduction. *Macromolecules* **2007**, *40*, 4446−4455.
(46) Lin, H.-W.; Lin, C.-L.; Chang, H.-H.; Lin, Y.-T.; Wu, C.-C.; Chen, Y.-M.; Chen, R.-T.; Chien, Y.-Y.; Wong, K.-T. Anisotropic Optical Properties and Molecular Orientation in Vacuum-Deposited Ter(9,9-diarylfluorene)s Thin Films Using Spectroscopic Ellipsometry. *J. Appl. Phys.* **2004**, *95*, 881−886.
(47) Gujral, A.; O'Hara, K. A.; Toney, M. F.; Chabinyc, M. L.; Ediger, M. D. Structural Characterization of Vapor-Deposited Glasses of an Organic Hole Transport Material with X-ray Scattering. *Chem. Mater.* **2015**, *27*, 3341−3348.
(48) Hüttner, S.; Sommer, M.; Steiner, U.; Thelakkat, M. Organic Field Effect Transistors from Triarylamine Side-chain Polymers. *Appl. Phys. Lett.* **2010**, *96*, No. 073503.
(49) Müller, D. C.; Braig, T.; Nothofer, H.-G.; Arnoldi, M.; Gross, M.; Scherf, U.; Nuyken, O.; Meerholz, K. Efficient Blue Organic Light-Emitting Diodes with Graded Hole-Transport Layers. *ChemPhysChem* **2000**, *1*, 207−211.
(50) Yang, X.; Müller, D. C.; Neher, D.; Meerholz, K. Highly Efficient Polymeric Electrophosphorescent Diodes. *Adv. Mater.* **2006**, *18*, 948−954.
(51) Chu, T.-Y.; Song, O.-K. Hole Mobility of *N*,*N*′-Bis(naphthalen-1-yl)-*N*,*N*′-bis(phenyl) benzidine Investigated by Using Space-Charge-Limited Currents. *Appl. Phys. Lett.* **2007**, *90*, No. 203512.
(52) Uoyama, H.; Goushi, K.; Shizu, K.; Nomura, H.; Adachi, C. Highly Efficient Organic Light-emitting Diodes from Delayed fluorescence. *Nature* **2012**, *492*, 234−238.
(53) Feuillastre, S.; Pauton, M.; Gao, L.; Desmarchelier, A.; Riives, A. J.; Prim, D.; Tondelier, D.; Geffroy, B.; Muller, G.; Clavier, G.; Pieters, G. Design and Synthesis of New Circularly Polarized Thermally Activated Delayed Fluorescence Emitters. *J. Am. Chem. Soc.* **2016**, *138*, 3990−3993.
(54) Li, C.; Nobuyasu, R. S.; Wang, Y.; Dias, F. B.; Ren, Z.; Bryce, M. R.; Yan, S. Solution-Processable Thermally Activated Delayed Fluorescence White OLEDs Based on Dual-Emission Polymers with Tunable Emission Colors and Aggregation-Enhanced Emission Properties. *Adv. Opt. Mater.* **2017**, *5*, No. 1700435.
(55) Liu, H.; Song, S.; Chen, H.; Zhao, Z.; Xie, G.; Tang, B. Z. Novel Aggregation-Induced Delayed Fluorescence Luminogens for Vacuum-Deposited and Solution-Processed OLEDs with very small efficiency roll-offs. *Org. Electron.* **2021**, *99*, No. 106339.
(56) Cai, Z.; Wu, X.; Liu, H.; Guo, J.; Yang, D.; Ma, D.; Zhao, Z.; Tang, B. Z. Realizing Record-High Electroluminescence Efficiency of 31.5% for Red Thermally Activated Delayed Fluorescence Molecules. *Angew. Chem., Int. Ed.* **2021**, *60*, 23635−23640.
(57) Wu, T.-L.; Huang, M.-J.; Lin, C.-C.; Huang, P.-Y.; Chou, T.-Y.; Chen-Cheng, R.-W.; Lin, H.-W.; Liu, R.-S.; Cheng, C.-H. Diboron Compound-based Organic Light-emitting Diodes with High Efficiency and Reduced Efficiency Roll-off. *Nature Photon.* **2018**, *12*, 235−240.
(58) Thesen, M. W.; Höfer, B.; Debeaux, M.; Janietz, S.; Wedel, A.; Köhler, A.; Johannes, H.-H.; Krueger, H. Hole-Transporting Host-Polymer Series Consisting of Triphenylamine Basic Structures for Phosphorescent Polymer Light-Emitting Diodes. *J. Polym. Sci., Part A: Polym. Chem.* **2010**, *48*, 3417−3430.
(59) Masui, K.; Nakanotani, H.; Adachi, C. Analysis of Exciton Annihilation in High-efficiency Sky-blue Organic Light-emitting Diodes with Thermally Activated Delayed Fluorescence. *Org. Electron.* **2013**, *14*, 2721−2726.
(60) Tonge, C. M.; Sauvé, E. R.; Cheng, S.; Howard, T. A.; Hudson, Z. M. Multiblock Bottlebrush Nanofibers from Organic Electronic Materials. *J. Am. Chem. Soc.* **2018**, *140*, 11599−11603.

https://doi.org/10.1021/jacs.2c00420
J. Am. Chem. Soc. 2022, 144, 8084−8095